Available online at www.sciencedirect.com
ScienceDirect
Journal of Solid State Chemistry 180 (2007) 1436–1445
JOURNAL OF SOLID STATE CHEMISTRY
www.elsevier.com/locate/jssc

Polymorphism in the $Sc_2Si_2O_7$–$Y_2Si_2O_7$ system

Alberto Escudero, María D. Alba, Ana. I. Becerro*

Departamento de Química Inorgánica, Instituto de Ciencia de Materiales de Sevilla, Universidad de Sevilla-CSIC, Avda. Américo Vespucio, s/n. 41092 Sevilla, Spain

Received 18 September 2006; received in revised form 1 November 2006; accepted 6 November 2006
Available online 2 December 2006

Abstract

This paper examines the structural changes with temperature and composition in the $Sc_2Si_2O_7$–$Y_2Si_2O_7$ system; members of this system are expected to form in the intergranular region of Si_3N_4 and SiC structural ceramics when sintered with the aid of Y_2O_3 and Sc_2O_3 mixtures. A set of different compositions have been synthesized using the sol–gel method to obtain a xerogel, which has been calcined at temperatures between 1300 and 1750 °C during different times. The temperature–composition diagram of the system, obtained from powder XRD data, is dominated by the β-$RE_2Si_2O_7$ polymorph, with γ-$RE_2Si_2O_7$ and δ-$RE_2Si_2O_7$ showing very reduced stability fields. Isotherms at 1300 and 1600 °C have been analysed in detail to evaluate the solid solubility of the components. Although, the XRD data show a complete solid solubility of β-$Sc_2Si_2O_7$ in β-$Y_2Si_2O_7$ at 1300 °C, the ^{29}Si MAS-NMR spectra indicate a local structural change at x ca. 1.15 ($Sc_{2-x}Y_xSi_2O_7$) related to the configuration of the Si tetrahedron, which does not affect the long-range order of the β-$RE_2Si_2O_7$ structure. Finally, it is interesting to note that, although $Sc_2Si_2O_7$ shows a unique stable polymorph (β), Sc^{3+} is able to replace Y^{3+} in γ-$Y_2Si_2O_7$ in the compositional range $1.86 \leqslant x \leqslant 2$ (where x is $Sc_{2-x}Y_xSi_2O_7$) as well as in δ-$Y_2Si_2O_7$ for compositions much closer to the pure $Y_2Si_2O_7$.

Keywords: Rare earth disilicate; Solid-state chemistry; Phase diagram; X-ray diffraction; MAS NMR

1. Introduction

When Si_3N_4 and SiC structural ceramics are sintered with the aid of *RE* oxides (*RE* = lanthanides, Y and Sc), a glassy *RE* disilicate phase ($RE_2Si_2O_7$) forms at the grain boundaries and, upon crystallization, the material shows improved high-temperature mechanical properties [1–9]. Knowledge of the crystalline structures adopted by the $RE_2Si_2O_7$ intergranular phase at different temperatures and *RE* contents is therefore of great value in understanding the behaviour of these materials. The high-temperature strength and oxidation resistance of Si_3N_4 and SiC are correlated with the cationic radius of the *RE* cation in the oxide additives, such that the smaller the *RE* cationic radius the better the properties of the ceramic [6,10]. Three *RE* oxides, Y_2O_3, Lu_2O_3 and Sc_2O_3, have shown the highest flexural strength values. This paper aims to examine the structures with temperature and composition in the $Sc_2Si_2O_7$–$Y_2Si_2O_7$ system; members of this system are expected to form in the intergranular region of Si_3N_4 and SiC structural ceramics when sintered with the aid of Y_2O_3 and Sc_2O_3 mixtures. Structural studies on the analogous $Lu_2Si_2O_7$–$Y_2Si_2O_7$ and $Sc_2Si_2O_7$–$Lu_2Si_2O_7$ systems have already been published by us [11–14].

The academic interest of these studies resides in the variety of polymorphic forms exhibited by the rare earth disilicates depending on the *RE* ionic radius, temperature and pressure [15,16]. $Y_2Si_2O_7$ shows up to five polymorphs with increasing temperature at room pressure (y, α, β, γ and δ, also called y, *B*, *C*, *D* and *E*, respectively) [16]; $Sc_2Si_2O_7$ exhibits, however, a unique polymorph (β or *C*) up to the melting point of the compound. The study of the $Sc_2Si_2O_7$–$Y_2Si_2O_7$ system is therefore interesting to analyse the stability fields of the different polymorphs with temperature and composition as well as to study the structural variations across the regions of solid solubility. Our previous study on the behaviour of the $Lu_2Si_2O_7$–

*Corresponding author. Fax: +34 95 446 06 65.
E-mail address: anieto@icmse.csic.es (A.I. Becerro).

0022-4596/$ - see front matter © 2007 Elsevier Inc. All rights reserved.
doi:10.1016/j.jssc.2006.11.029

$Y_2Si_2O_7$ system will allow establishing and explaining similarities and differences between both systems.

2. Experimental

2.1. Synthesis

The sol–gel route used for this study was derived from the synthesis of a well-homogenized gel of $Y_2Si_2O_7$ [17]. The starting materials were $Y(NO_3)_3 \cdot 6H_2O$ (99.9% Sigma), $Sc(NO_3)_3 \cdot 3H_2O$ (99.999% Sigma), $Si(OC_2H_5)_4$ (TEOS, 98% solution Sigma) and 96% ethanol. A TEOS solution in ethanol (1:3 in volume) was added over appropriate amounts of $Y(NO_3)_3 \cdot 6H_2O$ and $Sc(NO_3)_3 \cdot 3H_2O$ previously dissolved in 5 mL ethanol for the preparation of $Sc_{2-x}Y_xSi_2O_7$ members with $x = 0$, 0.20, 0.40, 0.60, 1.00, 1.30, 1.50, 1.70, 1.86, 1.90, 1.94, 1.98 and 2.00. The mixtures were stirred at 40 °C until transparent gels were obtained. The gels were dried at 60 °C for 24 h in air. Nitrate was eliminated by calcination at 500 °C for 1 h at a heating rate of 1 °C min^{-1}. The white powder obtained was subsequently calcined at a heating rate of 5 °C min^{-1} up to 1300 °C for 24 h and slowly cooled down to room temperature. Samples with $x \geqslant 1.50$ were also calcined at 1400, 1500, 1600, 1650, 1700 and 1750 °C during variable times to study the thermodynamic stability of the polymorphs formed. Thermal treatments are summarized in Table 1.

2.2. Characterization

Routine X-ray diffraction (XRD) patterns were carried out using a Siemens D-501 diffractometer, with Ni-filtered Cu$K\alpha$ radiation, steps of 0.05° and counting time of 3 s. Additional XRD patterns were taken with steps of 0.02° and a counting time of 10 s, in order to calculate unit cell parameters using the Le Bail method with the GSAS software [18]. The background was previously subtracted automatically using the diffractometer software although background intensities were subsequently refined afterwards. Refined parameters were: background coefficients, phase fractions, lattice constants and isotropic temperature factors. Powder elemental silicon was used as internal standard.

^{29}Si Magic Angle Spinning Nuclear Magnetic Resonance (MAS-NMR) spectroscopy measurements were carried out in a Bruker DRX400 (9.39 T) spectrometer equipped with a multinuclear probe, using 4 mm zirconia rotors spinning at 11 kHz. A single-pulse sequence was used, with a pulse length of 2.5 μs ($\pi/2$ pulse length = 7.5 μs), an observation frequency for ^{29}Si of 79.49 MHz, and an optimized delay time of 600 s. The chemical shifts are reported in ppm from tetramethylsilane (TMS).

3. Results and discussion

3.1. Temperature–composition diagram

Table 1 summarizes the phases observed after annealing each composition at the temperatures and times indicated. Fig. 1a shows the temperature–composition diagram of the $Sc_2Si_2O_7$–$Y_2Si_2O_7$ system obtained from the data in Table 1. The boundaries of adjacent stability field are based on data obtained from the synthesis of the compounds. The transition temperatures of the polymorphs, obtained from annealing experiments in which each phase is intended to be converted into the other, might differ slightly from these data. Fig. 1a shows that the (β phase is the stable one for

Table 1
$Sc_{2-x}Y_xSi_2O_7$ polymorphs obtained after calcination of the xerogels at different temperatures and times

T (°C) and time	x ($Sc_{2-x}Y_xSi_2O_7$)												
	0.00	0.20	0.40	0.60	1.00	1.30	1.50	1.70	1.86	1.90	1.94	1.98	2.00
1300 24 h	β	β	β	β	β	β	β	β	β	β	β	β	β
1400 24 h	β	β	β	β	β	β	β	β	β	$\beta+(\gamma)$	$\beta+\gamma$	$\gamma+\beta$	$\gamma+\beta$
1500 24 h									$\beta+(\gamma)$	$\gamma+(\beta)$	$\gamma+\beta$	$\gamma+(\beta)$	$\gamma+(\beta)$
4 d									$\gamma+\beta$		γ		
1600 24 h									γ	γ	γ	γ	γ
1650 24 h						β	β	β	γ	γ	γ	$\gamma+(\delta)$	$\gamma+(\delta)$
1700 12 h						β	β	β	γ		γ		
24 h						β	β	β	γ		γ		
1750 12 h							β	β	γ		γ		δ

All treatments refer to 24 h, except the ones indicated. In the case of two polymorphs, the one written in the first place is the most abundant. Brackets indicate traces. $\beta = \beta$-$Sc_{2-x}Y_xSi_2O_7$, $\gamma = \gamma$-$Sc_{2-x}Y_xSi_2O_7$ and $\delta = \delta$-$Sc_{2-x}Y_xSi_2O_7$.

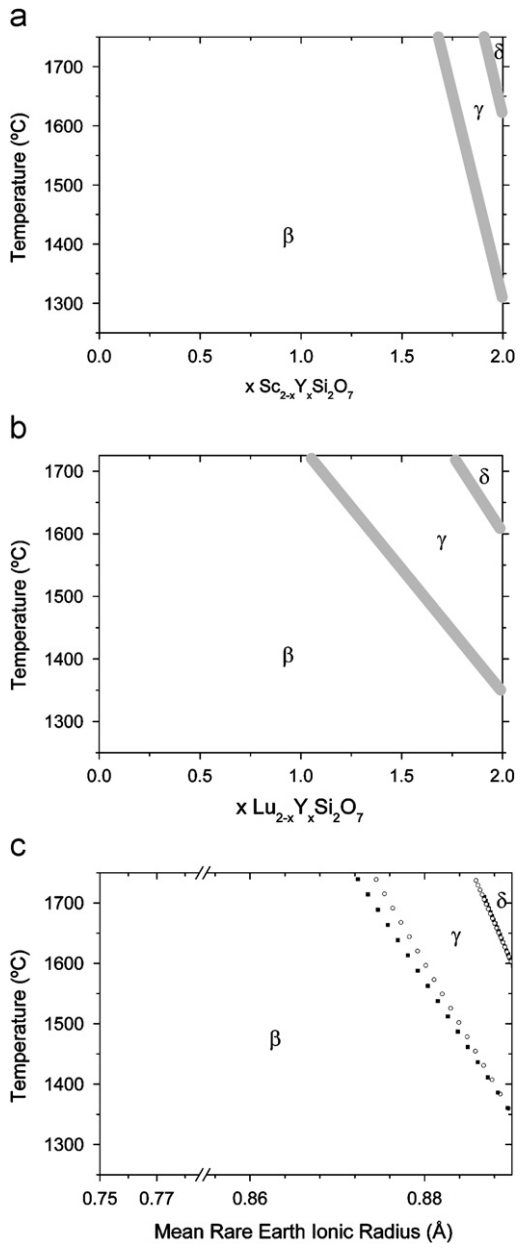

Fig. 1. (a) Temperature–composition diagram of the $Sc_2Si_2O_7$–$Y_2Si_2O_7$ system based on the data of Table 2. (b) Temperature–composition diagram of the $Lu_2Si_2O_7$–$Y_2Si_2O_7$ system, as reported in Ref. [13]. (c) Observed stable disilicate phases as a function of mean rare earth ionic radius.

all compositions with $x \leqslant 1.70$ at any temperature. The wide range of stability of this structure type is likely to be explained by the nearly closest hexagonal packing of the oxygen containing rare earth cations in octahedral holes and silicons in tetrahedral holes in alternating parallel layers (001). For compositions with $x \geqslant 1.86$ a narrow stability field of the γ-polymorph can be observed with a very pronounced slope separating it from the β field. Finally, the highest temperature phase δ is only observed for compositions with $x > 1.98$ at temperatures higher than 1650 °C.

The diagram is similar to the one reported by us for the $Lu_2Si_2O_7$–$Y_2Si_2O_7$ system [13] and reproduced here in Fig. 1b; both systems share one end-member ($Y_2Si_2O_7$) while the other ($Lu_2Si_2O_7$ or $Sc_2Si_2O_7$) shows a unique polymorph at any temperature, the β-polymorph in both cases. Therefore, the similarity between both temperature–composition diagrams is not surprising. The main difference between them is the width of the β-field, which is narrower in the $Lu_{2-x}Y_xSi_2O_7$ system, with a β-γ transition composition at x ca. 1.00 at 1700 °C, to be compared to $x = 1.70$ in the $Sc_{2-x}Y_xSi_2O_7$ system at the same temperature. The reason very likely resides on the different ionic radii of Sc^{3+} (0.745 Å) and Lu^{3+} (0.861 Å) compared to Y^{3+} (0.890 Å) [19]; the similar ionic radii of Lu^{3+} and Y^{3+} allows high concentrations of Lu^{3+} entering the *RE* crystallographic site of the γ-$RE_2Si_2O_7$ structure, even when the β-polymorph is the only one which is stable in pure $Lu_2Si_2O_7$. However, the smaller size of Sc^{3+} compared to Y^{3+} destabilizes the γ-$RE_2Si_2O_7$ structure even at very low Sc contents, and the transformation into the shared β-$RE_2Si_2O_7$ polymorph takes place. In fact, Fig. 1c shows that the stability range of the polymorphs obeys the mean rare earth radius, as established by Felsche [16].

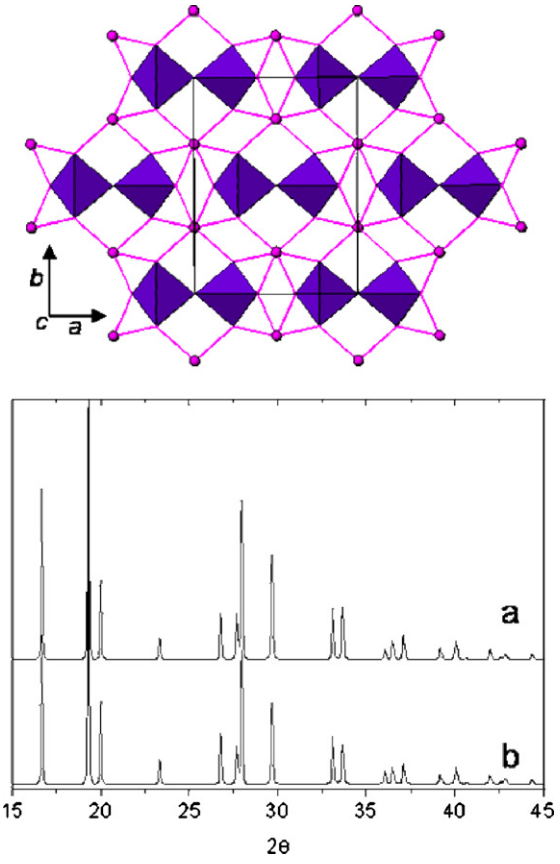

Fig. 2. Top: The crystal structure of β-$RE_2Si_2O_7$ with $C2/m$ symmetry (SiOSi angle = 180°). A very similar structure is observed in the case of $C2$ symmetry, but the SiOSi angle < 180°. The double tetrahedra correspond to $[Si_2O_7]^{6-}$ units while the spheres represent the RE^{3+} cations. Bottom: Theoretical XRD patterns of β-$RE_2Si_2O_7$ using $C2$ (plot a) and $C2/m$ (plot b), showing the same set of reflections.

Following is a structural study of two isotherms (1300 and 1600 °C) of the temperature–composition diagram of Fig. 1a. At 1300 °C all compositions crystallize as β-$RE_2Si_2O_7$ while at 1600 °C the γ polymorph is the stable phase for compositions with $x \geqslant 1.86$.

3.2. Structural study of β-$Sc_{2-x}Y_xSi_2O_7$ samples ($x = 0$–2) at 1300 °C

The general structure of the β-$RE_2Si_2O_7$ pyrosilicates is based on $(Si_2O_7)^{6-}$ units formed by two Si tetrahedra sharing one corner and RE^{3+} cations occupying octahedral holes (Fig. 2, top) [16]. Two different space groups, with the same unit cell size, have been used in the literature to describe the β-$RE_2Si_2O_7$ crystal structure. One of them, $C2/m$ forces de SiOSi angle to be 180° although considerable motion of the bridging oxygen is indicated by the temperature factor value [20]; the other space group, $C2$, allows SiOSi angles different from 180° [21]. Fig. 2, bottom, displays theoretical XRD patterns corresponding to β-$RE_2Si_2O_7$ using space groups $C2/m$ and $C2$; the same set of reflections is observed in both patterns.

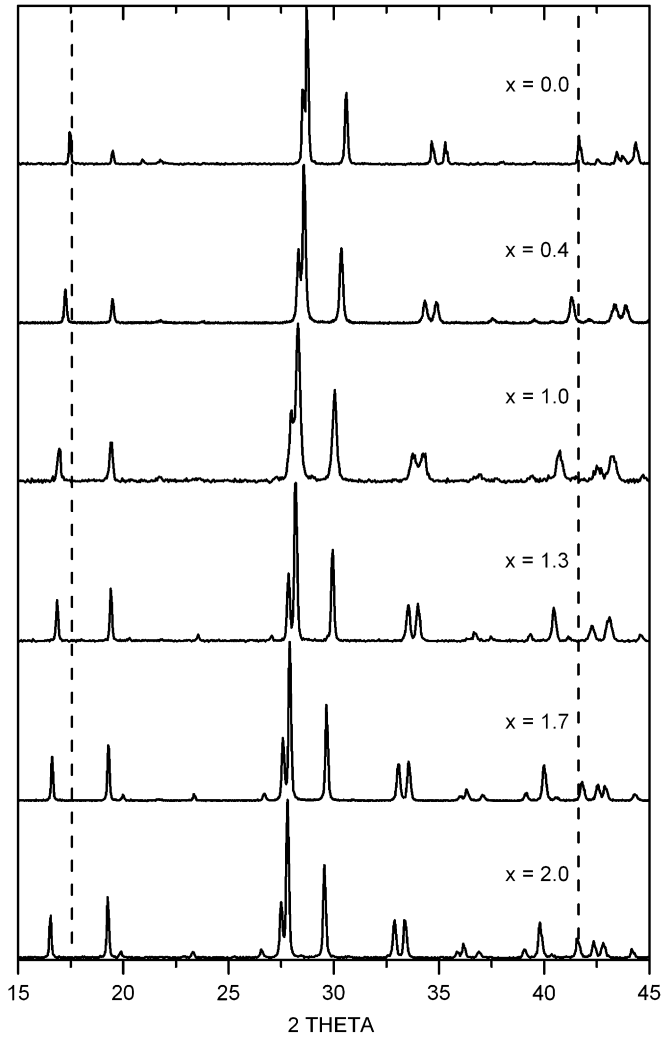

Fig. 3. Representative portions of the XRD patterns of samples in the $Sc_{2-x}Y_xSi_2O_7$ system with $x = 0.00$, 0.40, 1.00, 1.30, 1.70 and 2.00, calcined at 1300 °C for 24 h. Two lines have been drawn on top of three diffractions of the $x = 0.00$ pattern to appreciate their shift to lower angles with increasing Y content.

3.2.1. XRD study

Fig. 3 shows representative portions (15–45° 2θ) of the XRD patterns corresponding to selected samples of the $Sc_{2-x}Y_xSi_2O_7$ system calcined at 1300 °C for 24 h. The diagram of the $x = 0$ sample matches the standard pattern of β-$Sc_2Si_2O_7$, JPCDS 72-779. Increasing yttrium content produces very similar patterns, with variations in peak positions (see peaks under the vertical guide lines) and intensities (see for example peaks at ca. 17° and 19° 2θ), which result from changes in unit cell dimensions and composition. Finally, the XRD diagram of the $x = 2.0$ $Sc_{2-x}Y_xSi_2O_7$ sample matches the standard pattern of β-$Y_2Si_2O_7$ (JCPDS chart 38-0440). The long-range order structure of the β polymorph is, therefore, maintained across the $Sc_2Si_2O_7$–$Y_2Si_2O_7$ system at 1300 °C.

In order to obtain the variation of structural parameters with composition, the XRD patterns of all compositions were analysed using the Le Bail method with the GSAS software, as described in the experimental section. The starting parameters for the refinement of the structures with $x \leqslant 1$ have been taken from those reported for pure β-$Sc_2Si_2O_7$ [22] while the refinement of compositions with $x > 1$ was carried out from the parameters reported for pure β-$Y_2Si_2O_7$ [23]. In both cases, space group $C2/m$ has been used. Fig. 4 shows the experimental, fitted and difference diagram corresponding to the $Sc_{2-x}Y_xSi_2O_7$ sample with $x = 1.0$, as an example. The rest of fits are very similar to the one shown. All reflections can be fitted on the basis of the monoclinic cell corresponding to the β-$RE_2Si_2O_7$ structure. No extra-peaks can be observed, which indicates

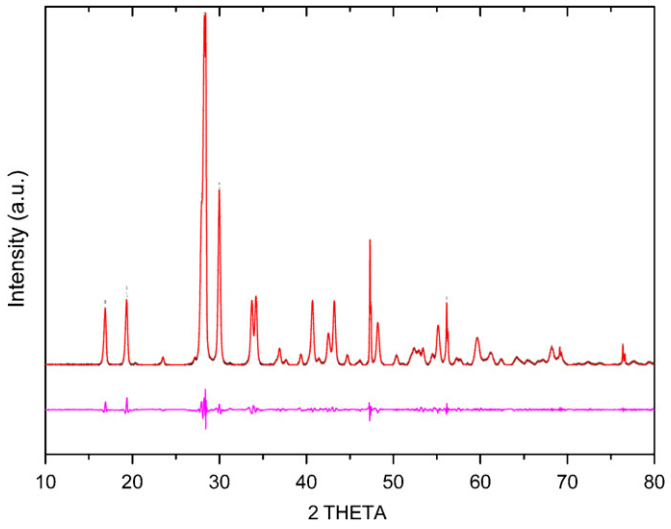

Fig. 4. Experimental (crosses) and calculated (solid line) XRD patterns of the $x = 1.00$ $Sc_{2-x}Y_xSi_2O_7$ sample annealed at 1300 °C for 24 h. The difference plot is also shown.

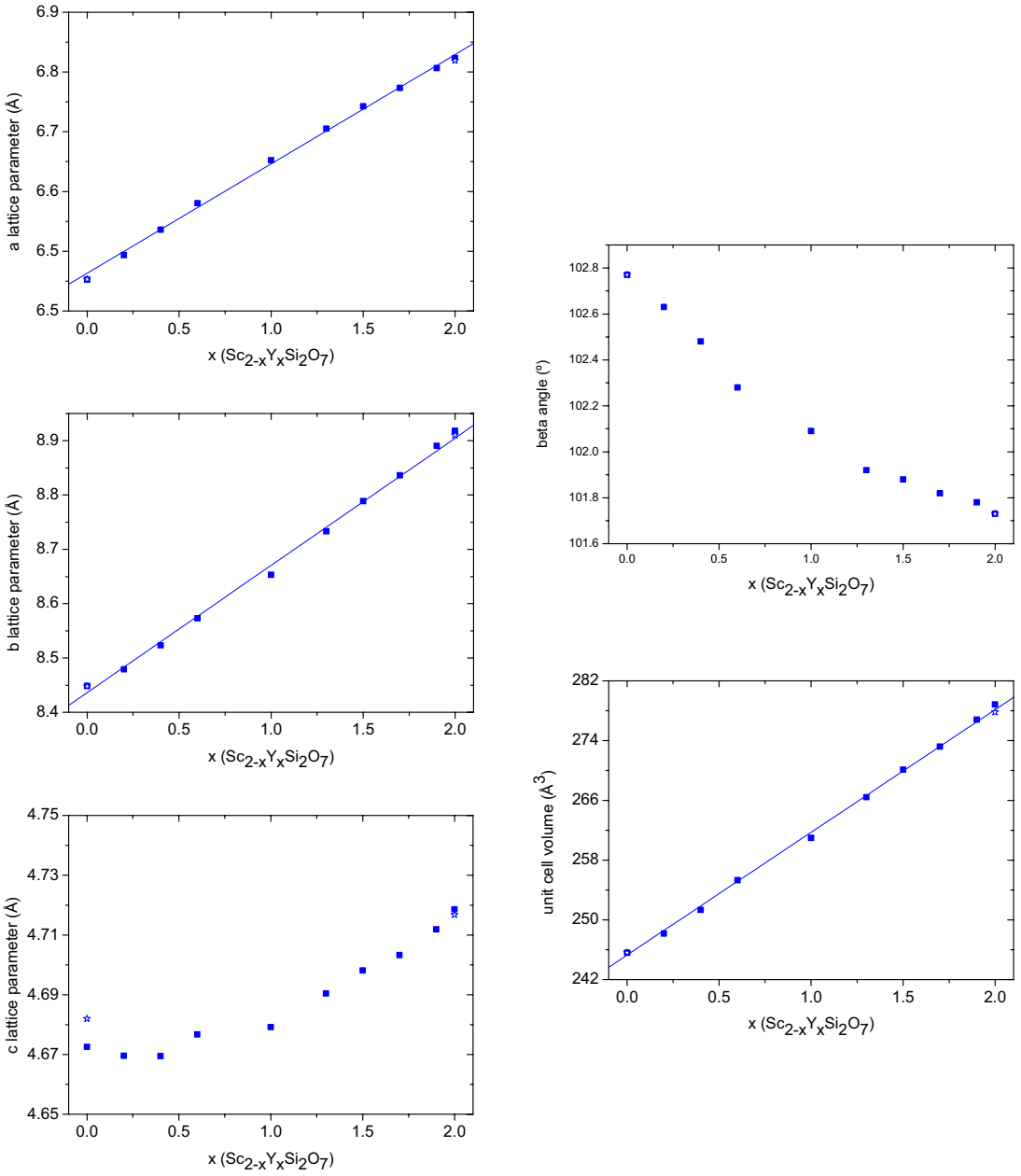

Fig. 5. Unit cell parameters (a, b, c, β and volume) plotted as a function of Y content corresponding to $Sc_{2-x}Y_xSi_2O_7$ samples annealed at 1300 °C for 24 h. The error bars are approximately the size of the symbols. The stars are the values found in the literature for the end-members β-$Sc_2Si_2O_7$ and β-$Y_2Si_2O_7$. Volume varies with composition as: Vol = 244.98 + 16.69x.

the absence of phase segregation. Fig. 5 shows the variation of the unit cell parameters with composition in the $Sc_{2-x}Y_xSi_2O_7$ system at 1300 °C. Most of the unit cell parameter values differ substantially from one end-member to the other due to the different ionic radii of Y^{3+} and Sc^{3+} [19]. Both a and b unit cell parameters increase linearly (around 5% from the sample with $x = 0$ to the sample with $x = 2$) with increasing yttrium content. The c unit cell parameter of pure β-$Sc_2Si_2O_7$ is very similar to that of pure β-$Y_2Si_2O_7$ (the variation from one to the other being <0.75%); however, a change in the slope can be observed at x ca. 1.0 when the c parameter is plotted versus Y content. A very small variation in the β angle value is also observed from one end-member to the other (<1%), although a change in slope also takes place here at x ca 1.0. The unit cell volume increases linearly when increasing yttrium content. The linearity of the data indicates the existence of a complete substitutional solid solution between β-$Sc_2Si_2O_7$ and β-$Y_2Si_2O_7$ at 1300 °C.

3.2.2. *^{29}Si MAS NMR study*

Fig. 6 shows the ^{29}Si MAS NMR spectra of the samples in the $Sc_{2-x}Y_xSi_2O_7$ system calcined at 1300 °C for 24 h. All of them show a unique band in the ppm range

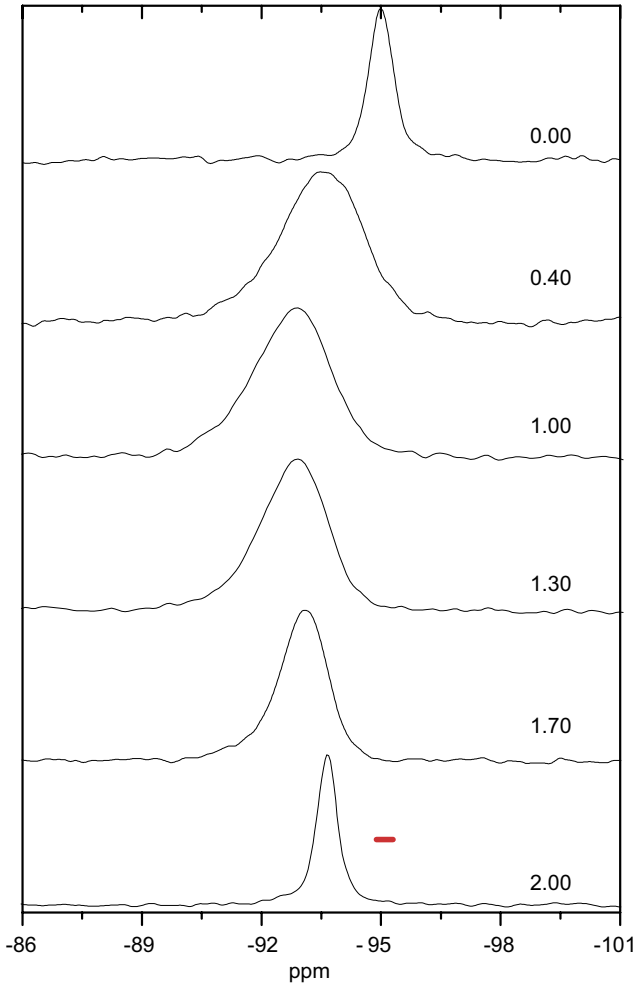

Fig. 6. ^{29}Si MAS NMR spectra of samples in the $Sc_{2-x}Y_xSi_2O_7$ system with $x = 0.00$, 0.40, 1.00, 1.30, 1.70 and 2.00, calcined at 1300 °C for 24 h.

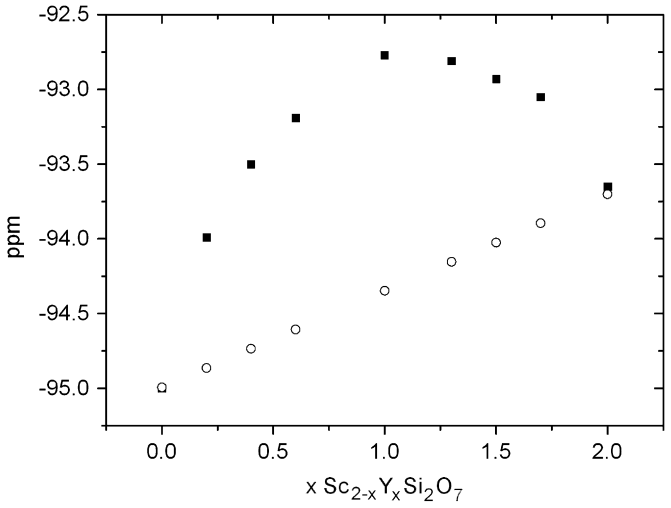

Fig. 7. Solid squares: ^{29}Si chemical shift values (in ppm) of samples in the $Sc_{2-x}Y_xSi_2O_7$ system versus Yttrium content. Open circles: ^{29}Si chemical shift values (in ppm) calculated from Janes and Oldfield's correlation using a SiOSi angle of 180°.

Table 2
^{29}Si chemical shift values (δ) and SiOSi angles obtained from the ^{29}Si chemical shift values using Janes and Oldfield correlations for the β-$Sc_{2-x}Y_xSi_2O_7$ structures (samples calcined at 1300 °C)

x ($Sc_{2-x}Y_xSi_2O_7$)	δ (ppm)	SiOSi angle (°)
0.0	−95.0	180.0
0.2	−94.0	174.8
0.4	−93.5	172.8
0.6	−93.1	171.4
1.0	−92.7	170.8
1.3	−92.8	172.6
1.5	−92.9	174.0
1.7	−93.1	175.9
2.0	−93.7	180.0

Spectral resolution is 0.1 ppm.

characteristic of the Q^1 environments of the $[Si_2O_7]^{6-}$ units in the pyrosilicate structure [24]. ^{29}Si chemical shifts values have been plotted versus composition in Fig. 7 and are given in Table 2. The values of the end members are in agreement with those reported in the literature for β-$Sc_2Si_2O_7$ [25] and β-$Y_2Si_2O_7$ [26]. The behaviour of the chemical shift values with composition is clearly nonlinear, with a maximum at x ca. 1.0, which is the composition at which, the line describing the c and β unit cell parameters behaviour bends. It seems, therefore, that there exists a relationship between the ^{29}Si chemical shift behaviour and the bending of the c and β unit cell parameters observed in the β-$Sc_{2-x}Y_xSi_2O_7$ system. The structural change producing the bending of the c and β unit cell parameters must be related to the close environment of Silicon, i.e. to the structure of the Si tetrahedra.

Janes and Oldfield [27] proposed a ^{29}Si chemical shift correlation based on group electronegativity, which applies successfully to pyrosilicate structures [12,14]. For type P silicon sites (all ligands being capable of sigma and pi bonding), as is the case of our pyrosilicate $Sc_{2-x}Y_xSi_2O_7$ structures, Janes and Oldfield give the following correlation:

$$\delta_{Si} = -24.336 \sum EN + 279.27, \quad (1)$$

where $\sum$EN is the group electronegativity sum of the various oxy-metal fragments to which Si is bonded in the pyrosilicate structure, i.e. OSi, OY and OSc in our system. Janes and Oldfield [27] derived the OSi group electronegativity as a function of bridging bond angle (SiOSi) obtaining the following equation:

$$EN(OSi) = (\angle SiOSi/136.79) + 2.9235. \quad (2)$$

On the other hand, group electronegativity values for OY and OSc have been empirically calculated by us in two previous papers, obtaining a value of 3.69 for OY [12] and of 3.71 for OSc [14]. We have used these equations to calculate the ^{29}Si chemical shifts across the $Sc_2Si_2O_7$–$Y_2Si_2O_7$ system, assuming a SiOSi angle of 180°. The data

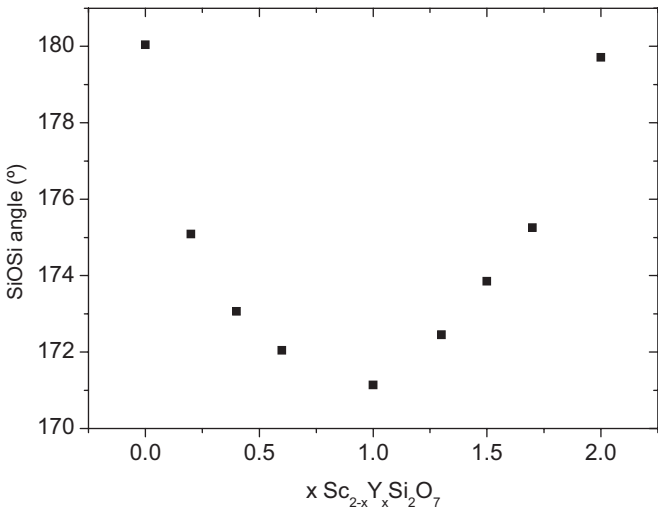

Fig. 8. SiOSi angle (°) calculated from Janes and Oldfield's correlation using the experimental ^{29}Si chemical shift values, plotted as a function of the Yttrium content.

have been plotted versus composition in Fig. 7. A clear mismatch between the experimental and the calculated values is observed which indicates that the SiOSi angle must differ from 180° across the system.

In order to calculate the SiOSi angle in the intermediate members of the $Sc_2Si_2O_7$–$Y_2Si_2O_7$ system, we have applied the Janes and Oldfield's correlation using the experimental ^{29}Si chemical shift values given in Table 2. The result is plotted in Fig. 8. It is observed that the SiOSi angle varies with composition, with a minimum of 170.8° at around the composition at which the c and β unit cell parameters change slope. In summary, the SiOSi angle of the double Si tetrahedra (Si_2O_7 unit) changes across the $Sc_2Si_2O_7$–$Y_2Si_2O_7$ system in order to accommodate the different sized Sc^{3+} and Y^{3+} in the octahedral holes of the pyrosilicate structure. This result implies that the space group of the intermediate members is $C2$ rather than $C2/m$, as is the case for the end-members. In any case, the unit cell size is the same and we have not recalculated it.

3.3. Structural study of γ-$Sc_{2-x}Y_xSi_2O_7$ samples ($1.86 \leqslant x \leqslant 2$) at 1600 °C

3.3.1. XRD study

Fig. 9 shows the XRD patterns of the $Sc_{2-x}Y_xSi_2O_7$ samples with $1.86 \leqslant x \leqslant 2$ annealed at 1600 °C for 24 h. Samples with $x < 1.86$ annealed in the same conditions crystallize as β-$RE_2Si_2O_7$ while only samples with $x \geqslant 1.86$ crystallize as γ-$RE_2Si_2O_7$. The diagram of the sample with $x = 2$ matches the standard pattern of γ-$Y_2Si_2O_7$, JPCDS 42-167, as expected. Decreasing yttrium content produces very similar patterns, with variations in peak positions and intensities, which result from changes in unit cell dimensions and compositions. No signs of phase segregation are observed which indicates that even though pure $Sc_2Si_2O_7$ forms a unique polymorph in the whole temperature range

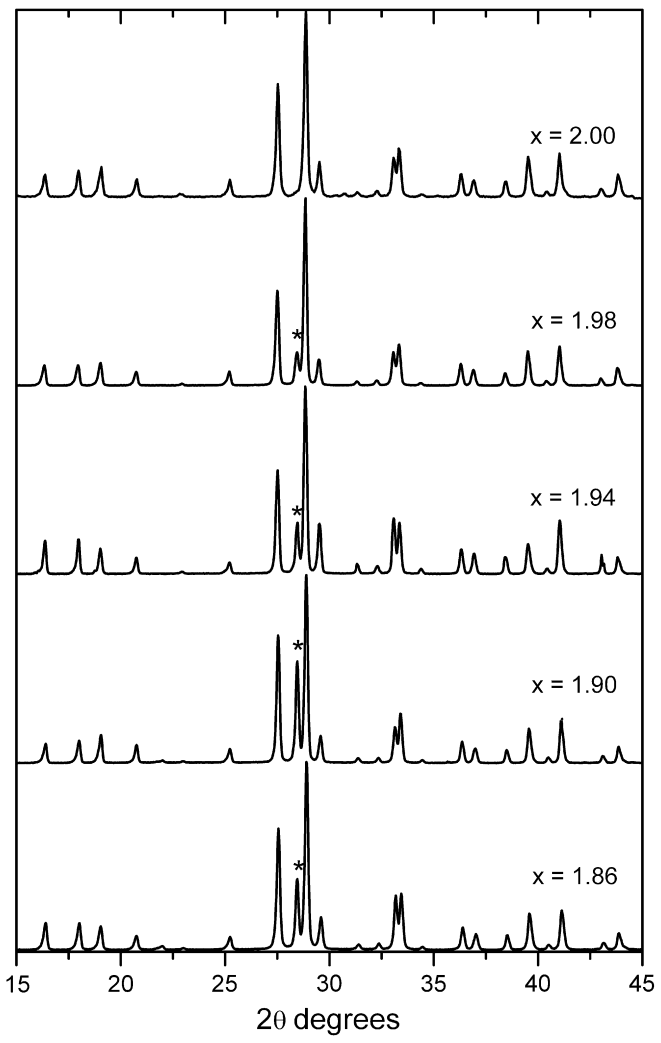

Fig. 9. Representative portions of the XRD diagrams of $Sc_{2-x}Y_xSi_2O_7$ samples with $x = 1.86$, 1.90, 1.94, 1.98 and 2.0, calcined at 1600 °C for 24 h. The asterisk indicates Si used for calibration.

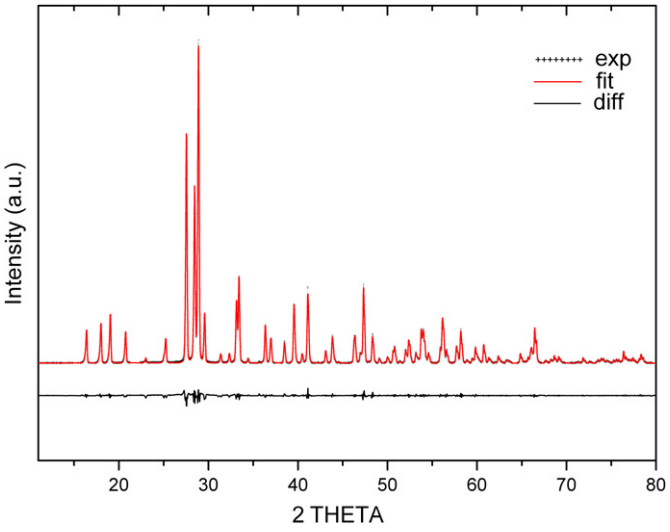

Fig. 10. Experimental (crosses) and calculated (dotted line) XRD patterns of the $x = 1.90$ $Sc_{2-x}Y_xSi_2O_7$ sample annealed at 1600 °C for 24 h. The difference plot is also shown.

(β), there is some degree of solid solubility of $Sc_2Si_2O_7$ in γ-$Y_2Si_2O_7$, i.e. Sc^{3+} is able to replace Y^{3+} in the pyrosilicate while maintaining the γ-structure in the compositional range $1.86 \leqslant x \leqslant 2$.

To confirm the solid solubility of $Sc_2Si_2O_7$ in γ-$Y_2Si_2O_7$ in the compositional range $1.86 \leqslant x \leqslant 2$ at 1600 °C, we have calculated the unit cell parameters of samples in Fig. 9 using the Le Bail method, as described in the experimental section. Starting unit cell parameters where those reported for pure γ-$Y_2Si_2O_7$ [28]. Fig. 10 shows the experimental, fitted and difference diagrams of the $x = 1.90$ composition, as an example. The rest of the XRD fits are very similar to the one shown. It can be observed that all reflections could be fitted on the basis on a monoclinic cell with space group $P2_1/c$, corresponding to the γ-$RE_2Si_2O_7$ structure.

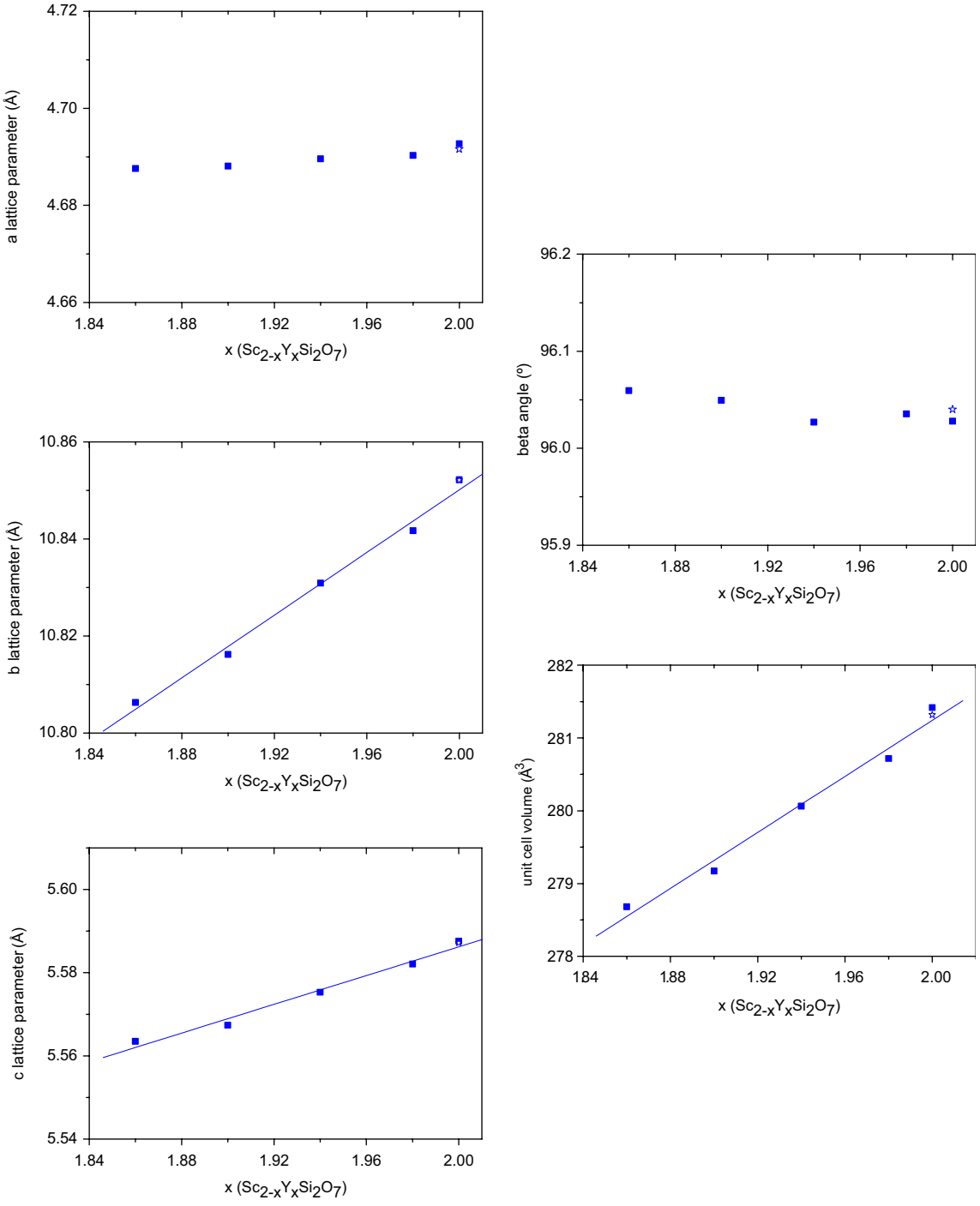

Fig. 11. Unit cell parameters (a, b, c, β and volume) plotted as a function of Y content corresponding to $Sc_{2-x}Y_xSi_2O_7$ samples annealed at 1600 °C for 24 h. The error bars are approximately the size of the symbols. The stars are the values found in the literature for the end-member γ-$Y_2Si_2O_7$. Volume varies with composition as: Vol = 242.77 + 19.23x.

The variation of unit cell parameters with composition is shown in Fig. 11. It is worth noting that we are dealing here with a narrow compositional range and, therefore, the variation of the unit cell values from one end to the other will be very small in comparison with the variation observed in the β structures. The same size of the y-axis has been used in the three plots to appreciate relative changes in the a, b and c unit cell parameters. The b and c unit cell parameters as well as the unit cell volume increase linearly with increasing yttrium content, while the a unit cell parameter and the β angle remain almost constant with composition. The linear behaviour of the unit cell parameters indicates the solid solubility of Sc in γ-$Y_2Si_2O_7$ in the $1.86 \leqslant x \leqslant 2$ compositional ranges and 1600 °C.

3.3.2. ^{29}Si MAS NMR study

Fig. 12 shows the ^{29}Si MAS NMR spectra of samples in the $Sc_{2-x}Y_xSi_2O_7$ system with $1.86 \leqslant x \leqslant 2$ calcined at 1600 °C for 24 h. Sample with $x = 2.00$ shows the narrowest curve, corresponding to a unique type of Si environment (Si surrounded by –OY groups). Decreasing yttrium content produces wider bands due to the presence of different Si environments (Si surrounded by –OY and –OSc groups). The ^{29}Si chemical shift value obtained for the $x = 2.00$ sample is in agreement with the value reported in the literature for γ-$Y_2Si_2O_7$ [26]. Decreasing yttrium content produces a slight shift of the values towards higher frequencies. Comparison of the behaviour of the ^{29}Si chemical values corresponding to γ-$RE_2Si_2O_7$ polymorphs with those of Fig. 7 (corresponding to β-$RE_2Si_2O_7$ polymorphs) is not possible due to the short compositional range in the case of the γ-$RE_2Si_2O_7$ polymorphs.

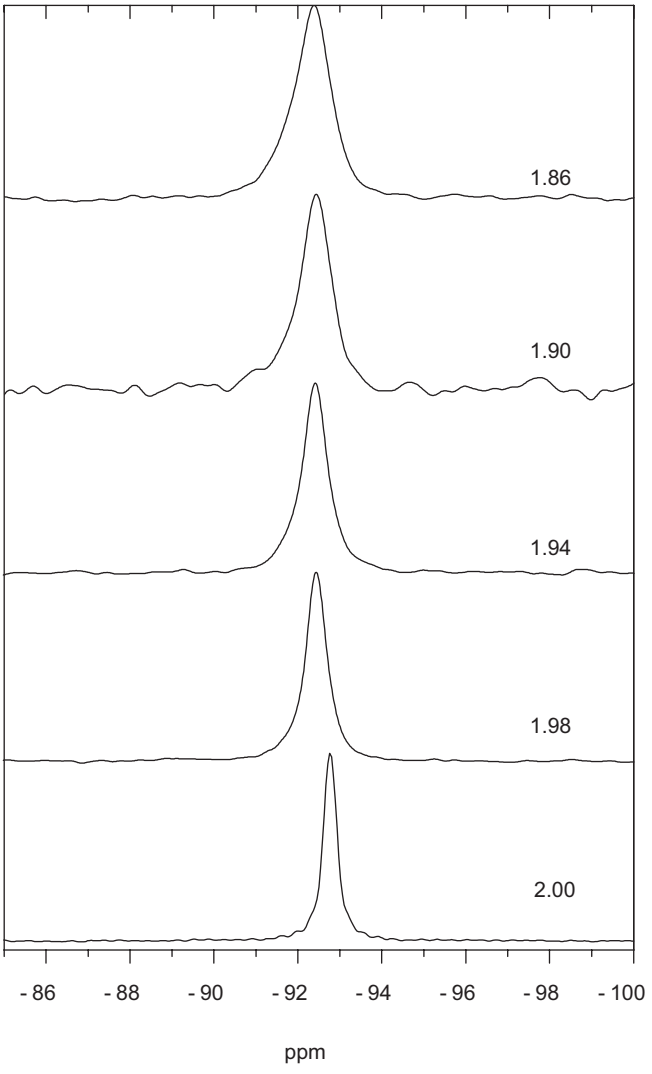

Fig. 12. ^{29}Si MAS NMR spectra of samples in the $Sc_{2-x}Y_xSi_2O_7$ system with $x = 1.86$, 1.90, 1.94, 1.96 and 2.00, calcined at 1600 °C for 24 h.

4. Conclusions

The results of the XRD and ^{29}Si MAS NMR analysis indicate that the $Sc_2Si_2O_7$–$Y_2Si_2O_7$ temperature–composition diagram is dominated by the β-$RE_2Si_2O_7$ polymorph, as previously observed for the $Lu_2Si_2O_7$–$Y_2Si_2O_7$ system. However, in this case, the γ and δ fields are much smaller due to the bigger difference in ionic radius between Y^{3+} and Sc^{3+} as compared to Y^{3+} and Lu^{3+}. It is important to note that, although the XRD data show a complete solid solubility of β-$Sc_2Si_2O_7$ in β-$Y_2Si_2O_7$ at 1300 °C, a minor structural change occurs at x ca. 1.00 ($Sc_{2-x}Y_xSi_2O_7$) related to the configuration of the Si tetrahedra, which does not affect the long-range order of the β-$RE_2Si_2O_7$ structure.

Acknowledgments

We gratefully acknowledge financial support from DGICYT Projects no. CTQ2004-05113 and Ramón y Cajal no. 2002/969. Likewise, EC is acknowledge for the project funded within the 6th Framework Programme as an HRM Activity under contract number MRTN-CT-2006-035957. A. Escudero thanks Ministerio de Educación y Ciencia for a FPU grant. 'High-temperature experiments were performed at the Bayerisches Geoinstitut under the EU "Research Infrastructures: Transnational Access" Programme (Contract No. 505320 (RITA)—High Pressure).

References

[1] A. Tsuge, K. Nishida, M. Komatse, J. Am. Ceram. Soc. 58 (1975) 323.
[2] C.H. Drummond, W.E. Lee, W.A. Sanders, J.D. Kiser, Ceram. Eng. Sci. Proc. 9 (1988) 1343.
[3] T.R. Dinger, R.S. Rai, G. Thomas, J. Am. Ceram. Soc. 71 (1988) 236.
[4] I.H. Arita, D.S. Wilkinson, G.R. Purdy, J. Am. Ceram. Soc. 75 (1992) 3315.
[5] P. Vomacka, O. Babushkin, J. Eur. Ceram. Soc. 15 (1995) 921.
[6] Z.L. Hong, H. Yoshida, Y. Ikuhara, T. Sakuma, T. Nishimura, M. Mitomo, J. Eur. Ceram. Soc. 22 (2002) 527.
[7] T. Yano, D.C. Park, Y. Horie, H. Inoue, K. Katayama, T. Iseki, Adv. Ceram. Comp. Key Eng. Mater. 247 (2003) 165.

[8] K.P. Plucknett, H.T. Lin, J. Am. Ceram. Soc. 88 (2005) 3538.
[9] K. Houjou K, K. Ando, M.C. Chu, S.P. Liu, S. Sato, J. Eur. Ceram. Soc. 25 (2005) 559.
[10] H.J. Choi, J.G. Lee, Y.W. Kim, J. Mater. Sci. 32 (1997) 1937.
[11] A.I. Becerro, A. Escudero, Chem. Mater. 17 (2005) 112.
[12] A.I. Becerro, A. Escudero, J. Solid State Chem. 178 (2005) 1.
[13] A.I. Becerro, A. Escudero, J. Eur. Ceram. Soc. 26 (2006) 2293.
[14] H. Ohashi, M.D. Alba, A.I. Becerro, P. Chain, A. Escudero, J. Phys. Chem. Solids 68 (2007) 464.
[15] J. Ito, H. Johnson, Am. Miner. 53 (1968) 1940.
[16] J. Felsche, Struct. Bond. 13 (1973) 99.
[17] M. Díaz, I. García-Cano, S. Mello-Castanho, J.S. Moya, M.A. Rodríguez, J. Non-Cryst. Solids 289 (2001) 151.
[18] A.C. Larson, R.B. Von Dreele, GSAS: General Structural Analysis System, Los Alamos National Laboratory, Los Alamos, NM, The Regents of the University of California, 1994.
[19] The values for Sc and Lu correspond to the ionic radii of the RE^{3+} cations in octahedral coordination, which is the coordination of the RE^{3+} in the β- and γ-$RE_2Si_2O_7$ structures. Values taken from R.D. Shannon, Acta Crystalallogr. A32 (1976) 751; The ionic radius of Yttrium has been taken form M.J. Pomeroy, E. Nestor, R. Ramesh, S. Hampshire, J. Am. Ceram. Soc. 88 (2003) 875.
[20] Yu.I. Smolin, Yu.F. Shepelev, Acta Crystallogr. B 26 (1970) 484.
[21] Yu.I. Smolin, Yu.F. Shepelev, I.K. Butikova, Zh. Strukt. Khim. 12 (1971) 272.
[22] Y.I. Smolin, Y.F. Shepelev, A.P. Titov, Kristallografiya 17 (1972) 857.
[23] G.J. Redhammer, G. Roth, Acta Crystallogr. C 59 (2003) 1103.
[24] G. Engelhardt, D. Michel (Eds.), High Resolution Solid State NMR of Silicates and Zeolites, Wiley, New York, 1987.
[25] M. Magi, E. Lippmaa, A. Samoson, J. Phys. Chem. 88 (1984) 1518.
[26] J. Parmentier, P.R. Bodart, L. Audoin, G. Massouras, D.P. Thompson, R.K. Harris, P. Goursat, J.L. Bessons, J. Solid State Chem. 149 (2000) 16.
[27] N. Janes, E. Oldfield, J. Am. Chem. Soc. 107 (1985) 6769.
[28] N. Christensen, R.G. Hazell, A.W. Hewat, Acta Chem. Scand. 51 (1997) 37.